

RESEARCH ARTICLE

INORGANIC CHEMISTRY

Eliminating nonradiative decay in Cu(I) emitters: >99% quantum efficiency and microsecond lifetime

Rasha Hamze¹, Jesse L. Peltier², Daniel Sylvinson¹, Moonchul Jung¹, Jose Cardenas¹, Ralf Haiges¹, Michele Soleilhavoup², Rodolphe Jazzar², Peter I. Djurovich¹, Guy Bertrand², Mark E. Thompson^{1*}

Luminescent complexes of heavy metals such as iridium, platinum, and ruthenium play an important role in photocatalysis and energy conversion applications as well as organic light-emitting diodes (OLEDs). Achieving comparable performance from more-earth-abundant copper requires overcoming the weak spin-orbit coupling of the light metal as well as limiting the high reorganization energies typical in copper(I) [Cu(I)] complexes. Here we report that two-coordinate Cu(I) complexes with redox active ligands in coplanar conformation manifest suppressed nonradiative decay, reduced structural reorganization, and sufficient orbital overlap for efficient charge transfer. We achieve photoluminescence efficiencies >99% and microsecond lifetimes, which lead to an efficient blue-emitting OLED. Photophysical analysis and simulations reveal a temperature-dependent interplay between emissive singlet and triplet charge-transfer states and amide-localized triplet states.

Organometallic complexes of heavy metals often phosphoresce from high-energy, long-lived triplet states with high luminance efficiency, enabling applications ranging from photocatalysis (1) and chemo- and biosensing (2, 3) to dye-sensitized solar cells (4) and organic electronics (5, 6). By contrast, phosphorescence of typical organocopper complexes is inefficient (7, 8) compared to organo-Ir and organo-Pt phosphors (9). This difference largely stems from the rates of two intersystem crossing (ISC) processes. The spin-orbit coupling (SOC) parameter (ξ) that facilitates ISC is smaller for the Cu nucleus ($\xi = 857 \text{ cm}^{-1}$) than for heavier metals such as Ir and Pt ($\xi = 3909$ and 4481 cm^{-1} , respectively) (10). Therefore, the rate of ISC from the lowest excited singlet state (S_1) to the lowest triplet excited state (T_1) typically is on the order of 10^{10} to 10^{11} s^{-1} in Cu complexes (11, 12) as opposed to 10^{13} to 10^{14} s^{-1} in heavy metal complexes (13, 14). The rate of radiative ISC from T_1 to the ground state (S_0) is markedly slower in organocopper phosphors ($k = 10^3$ to 10^4 s^{-1}) compared to Ir and Pt emitters ($k > 10^5 \text{ s}^{-1}$) (5, 15). Moreover, the lowest-energy optical transitions in most Cu(I) complexes are typically metal-to-ligand charge transfer (MLCT) events, which are associated with large reorganization energies. In these MLCT transitions, formal oxidation at

the d^{10} metal center induces Jahn-Teller distortion (16) that not only increases nonradiative decay rates but also leads to ISC rates even slower than those expected based only on SOC considerations (17).

In the past decade, thermally assisted delayed fluorescence (TADF) has emerged as a useful alternative for harvesting both singlet and triplet excitons generated in organic light-emitting diodes (OLEDs) (18–21). This process is accomplished by bringing the S_1 and T_1 manifolds close enough in energy to give high rates for exo- and endothermic ISC between them. (Fig. 1A). The resulting equilibrium between S_1 and T_1 typically favors the longer-lived, weakly emissive triplet; however, a high radiative rate from S_1 can lead to a high radiative efficiency for the TADF process. A conundrum in purely organic, donor-acceptor-type TADF systems is raised by the opposing requirements for minimizing the energy gap between the two lowest excited states ($\Delta E_{S_1-T_1}$) through poor highest occupied molecular orbital (HOMO)–lowest unoccupied molecular orbital (LUMO) overlap and achieving high radiative rates for the S_1 state via large orbital overlap (22). TADF also occurs in Cu(I) complexes and was first observed by McMillin and co-workers (23). In such Cu complexes, the HOMO is typically metal-based, and the LUMO is composed of ligand π^* orbitals. However, Cu TADF systems present a major departure from their pure organic counterparts: Forward ISC in the Cu(I) compounds is fast enough to quantitatively depopulate the S_1 state, thereby completely outpacing prompt fluorescence and resulting in monoexponential

emission decay at all temperatures. To illustrate, a highly emissive Cu complex with the smallest recorded $\Delta E_{S_1-T_1} = 33 \text{ meV}$ has a radiative rate (k_r) of $2 \times 10^5 \text{ s}^{-1}$ in the solid state at room temperature (it is only weakly emissive in fluid solution) (20). Fitting the temperature-dependent photoluminescent decay of this complex to the modified Boltzmann Eq. 1, where k_{S_1} and k_{T_1} are the rate constants for radiative decay from the S_1 and T_1 states, respectively, k_B is Boltzmann's constant, and T is temperature, gives a derived rate of fluorescence (prompt emission from S_1) of $2 \times 10^6 \text{ s}^{-1}$ (24), which is a full order of magnitude faster than the recorded rate of emission (TADF) at room temperature. It is therefore reasonable to conclude that the limiting factor in determining the rate of TADF in Cu systems is the endothermic ISC from T_1 to S_1 , which is tied to SOC as shown in Eq. 2, where ρ_{FC} denotes the Frank-Condon density of states and $|\langle S_1 | \hat{H}_{SO} | T_1 \rangle|$ denotes the SOC matrix element (25). Nevertheless, even the most efficient TADF-based Cu emitters have low photoluminescence (PL) quantum yields (Φ_{PL}) in fluid or polymeric matrices. High rates of nonradiative decay are observed in nonrigid environments owing to substantial distortions in the excited state of frequently studied tetrahedral motifs (26, 27):

$$\tau_{\text{TADF}} = \frac{3 + \exp\left(\frac{\Delta E_{S_1-T_1}}{k_B T}\right)}{3k_{T_1} + k_{S_1} \exp\left(\frac{\Delta E_{S_1-T_1}}{k_B T}\right)} \quad (1)$$

$$k_{\text{ISC}} = \frac{2\pi}{\hbar} \rho_{\text{FC}} |\langle S_1 | \hat{H}_{SO} | T_1 \rangle|^2 \quad (2)$$

Reports of linear Cu complexes with high Φ_{PL} in nonrigid matrices highlight the appeal of low coordination in limiting excited-state reorganization (28–30). Unfortunately, the MLCT nature of the radiative transitions in these derivatives leads to excited-state lifetimes that are relatively long ($\tau \sim 20 \mu\text{s}$), thus limiting their luminescent efficiency. However, a recent paper by Di *et al.* has reported efficient green electroluminescence (EL) in OLEDs using two-coordinate carbene-gold and carbene-copper complexes [maximum external efficiency (EQE_{max}) = 26.3% for the former and 9.7% for the latter] (19). The complexes discussed by Di *et al.* consist of Au(I) or Cu(I) ions coordinated to a cyclic (alkyl)(amino)carbene (CAAC) (31, 32) and an N-bound amide. Here we examine a closely related family of two-coordinate, neutral CAAC-Cu(I)-amide complexes with notable photophysical properties (see Fig. 1; compound **1b** was examined by Di *et al.*). Optimizing the steric encumbrance of substituents on the carbene, we achieve complexes with $\Phi_{PL} > 99\%$ and short emission lifetimes ($\tau = 2$ to $3 \mu\text{s}$) in fluid and polymeric media. Electrochemical, photophysical, and computational analyses reveal a picture of ligand-based frontier orbitals with minimal metal contribution. Coplanar ligand conformation in these complexes is critical to maintaining high Φ_{PL} . Finally, one of the complexes is used in blue OLEDs.

¹Department of Chemistry, University of Southern California, Los Angeles, CA, USA. ²UCSD-CNRS Joint Research Laboratory (UMI 3555), Department of Chemistry and Biochemistry, University of California, San Diego, La Jolla, CA 92093-0358, USA.

*Corresponding author. Email: met@usc.edu

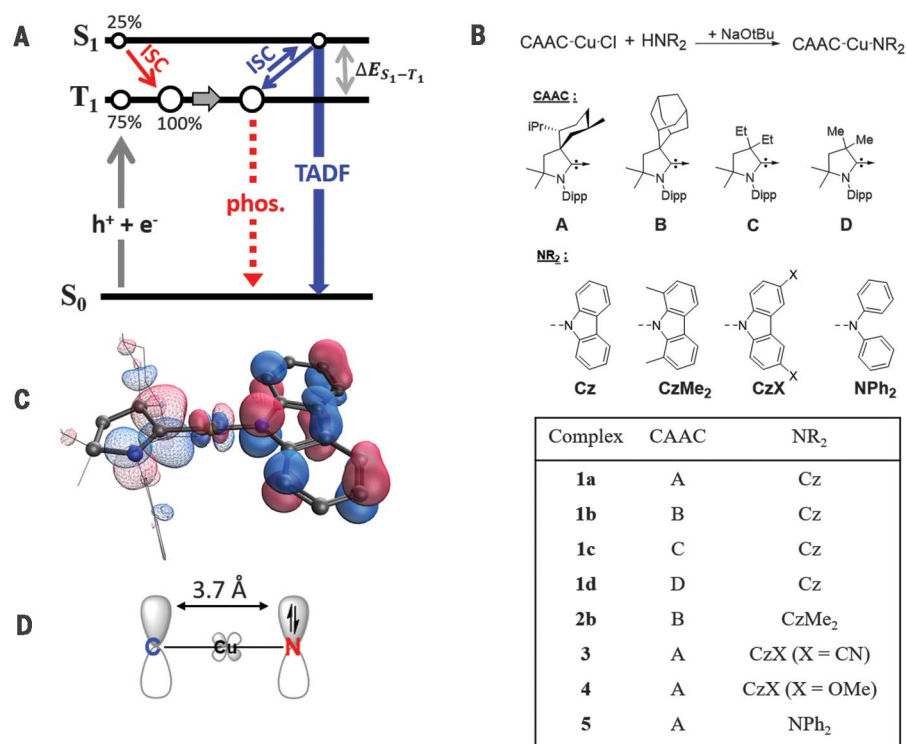


Fig. 1. Background and chemical structures of CAAC-Cu-amides. (A) Scheme depicting the radiative processes [phosphorescence (phos.) and TADF] in an OLED. (B) Complexes studied in this work. Dipp, 2,6-diisopropylphenyl; tBu, tert-butyl; iPr, isopropyl; Et, ethyl; Me, methyl. (C) HOMO (solid) and LUMO (mesh) surfaces of complex **1a**. (D) Simplified picture of the HOMO and LUMO of complex **1a**.

Structural and electronic properties of CAAC-Cu-amide complexes

The two-coordinate CAAC-Cu-amide complexes were prepared in high yields (80 to 90%) following literature procedures (Fig. 1B) (19). Complexes **1** to **5** were isolated as white to yellow powders and display varying degrees of sensitivity to O₂ and moisture depending on the steric bulk around the carbene and the nature of the amide. Complex **1b**, bearing 1,8-dimethyl carbazolidine (CzMe₂), was found to be highly sensitive to H₂O and CO₂ in ambient air as a solid and in solution (see the supplementary materials).

X-ray diffraction analysis was performed on single crystals of the complexes **1a**, **1c**, **1d**, **2b**, and **3** to **5** (see figs. S1 to S8 and tables S1 to S8). The structures all display a near-linear coordination geometry around the Cu center (174° to 179°), with a 3.73 to 3.77 Å separation between the carbene carbon and the amide nitrogen owing to similar bond lengths (C–Cu = 1.88 to 1.89 Å; Cu–N = 1.85 to 1.87 Å). Dihedral angles between the ligands are <9° in complexes **1a**, **1c**, **1d**, and **3** to **5**, whereas complex **2b** has a near orthogonal conformation (dihedral angle = 83°). Despite the asymmetry of the CAAC, only one set of ¹H NMR (nuclear magnetic resonance) spectroscopic resonances for the carbazolidine is observed in all complexes. This observation indicates rapid exchange on the NMR time scale, likely caused by rotation around the C_{carbene}–N_{amide} axis. Variable temperature NMR experiments performed on complex

1a down to –60°C show no signs of coalescence, which suggests a low energy barrier for the rotation in question. Complex **2b** also shows one set of carbazolidine resonances in its ¹H NMR spectrum, consistent with an orthogonal conformation for the ligands.

The electrochemical properties of the Cu complexes **1a** and **3** to **5**, precursors (CAAC^{Me}-CuCl, where CAAC^{Me} is ligand A in Fig. 1B, and the free amines), and potassium carbazolidine (KCz) were examined (see fig. S11 and table S11 for details). The Cu complexes undergo irreversible oxidation at potentials that vary over a 1-V range, depending on the donor strength of the amide ligand. Relative to their parent amines, the oxidation potentials of the Cu-amides decrease by 0.6 to 0.7 V. All potentials fall well below the Cu(I) oxidation potential of CAAC^{Me}-CuCl. The oxidation potential of **1a** is anodically shifted by 0.73 V compared to that of KCz, consistent with metalation. Reduction potentials are quasi-reversible, with values that are unchanged from the parent CAAC^{Me}-CuCl. The data show that the redox potentials are independently controlled by the ligands: Oxidation is primarily at the amide, and reduction at the π-accepting carbene.

The redox noninnocent nature of the ligands is also captured by density functional theory (DFT; B3LYP/LACVP**). As shown in Fig. 1C, the HOMO is principally amide-based, with substantial electron density residing in the filled p orbital of N_{amide}. The LUMO is localized largely

on the unfilled p orbital of C_{carbene}. The nature of the frontier molecular orbitals and coplanar orientation of the ligands allow for a simplified representation of the valence structure (Fig. 1D) as a donor-bridge-acceptor linear system, wherein the metal d orbitals act as a weak electronic bridge between the parallel donor (N_{amide} 2p_z) and acceptor (C_{carbene} 2p_z) orbitals, thereby illustrating the potential for long-range π interaction (33, 34). The ground state of these complexes is marked by a large permanent dipole, μ_g ~11.3 D, in close agreement with the report by Föllner and Marian for an isoelectronic Au complex (35).

Absorption spectra of complexes **1a**, **1b**, **2b**, and **3** to **5** in tetrahydrofuran (THF) (Fig. 2A) show high-energy bands (λ < 350 nm) corresponding to π-π* transitions of the ligands. Broad, low-energy bands apparent in these complexes are assigned to singlet interligand charge transfer (ICT) from the electron-rich amide to the electron-accepting carbene. The onset of the ICT bands for **1a** and **3** to **5** falls in the order expected based on the oxidation potentials of their amide ligands (inset of Fig. 2A). A notable feature of the ICT transitions in these complexes is their high extinction coefficients (ε > 10³ M⁻¹ cm⁻¹), which is surprising considering the ~3.7 Å separation between the HOMO and LUMO. These values are a factor of 10 greater than what is typically observed for MLCT transitions in organocopper complexes. We tentatively attribute the strongly allowed nature of the charge-transfer (CT) transitions in these complexes to the small but nonnegligible contribution of the Cu d orbitals acting as an effective electronic bridge between the donor and the acceptor components. In addition, the coplanarity of the ligands leads to a parallel orientation of the filled 2p_z orbital on the amide N and the empty 2p_z orbital on the carbene C, maximizing long-range orbital overlap.

A characteristic property of the ICT band in these complexes is the pronounced hypsochromic shift as solvent polarity increases (Fig. 2B). The absorption onset of the ICT band undergoes a blue shift of 2400 cm⁻¹ in **1a** and 2600 cm⁻¹ in **5** upon increasing solvent polarity. The magnitude of the shift reflects a strong change in the electronic dipole moment upon excitation. The direction of the shift is a consequence of the ground-state dipole being much larger in magnitude and opposite in orientation relative to its excited-state counterpart (36). Similar hypsochromic shifts of the ICT absorption band are observed upon freezing the solvent matrix and are more pronounced in methylcyclohexane (MeCy) than in 2-methyltetrahydrofuran (2-MeTHF) (Fig. 2C). The blue shift in 2-MeTHF at 77 K is likely due to the solvent dipoles being frozen around the large solute dipole, stabilizing the ground state (relaxing the potential energy surface) and destabilizing the ICT excited state. The blue shift recorded in MeCy at 77 K, where the solubility of **1a** is reduced, can be brought about by long-range dipole-dipole interactions between the solute molecules (37). In both instances, the hypsochromic shift is absent when the solvent glass is thawed.

Efficient luminescence from allowed interligand charge transfer transitions

The Cu complexes all luminesce with high efficiency in fluid solution, as well as when doped in polystyrene (PS) matrices, manifesting microsecond radiative lifetimes (Fig. 3A and Table 1). Pow-

dered samples of the carbazolid complexes **1a** to **1d** and **3** are poorly emissive, whereas **2b**, **4**, and **5** exhibit stronger luminescence in their microcrystalline forms than in solution (see figs. S22, S23, and S26 and table S15). Emission spectra of **1a** to **1d**, **4**, and **5** in 2-MeTHF solutions are

broad and featureless at room temperature, consistent with the ICT origin of these transitions. The PL efficiency improves as the steric encumbrance on the carbene increases in the series **1d** < **1c** < **1b** < **1a** ($\Phi_{\text{PL}} = 0.1, 0.6, 0.7$, and 1.0 , respectively). Because **1a** to **1d** have similar

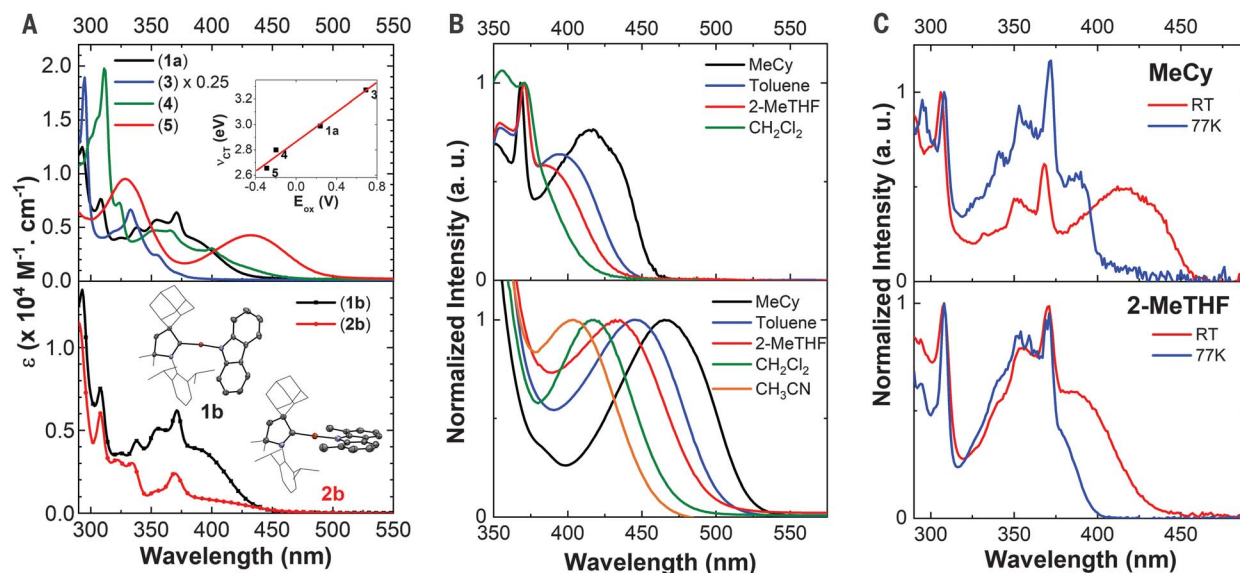


Fig. 2. Electronic spectra of CAAC-Cu-amides. (A) Absorption spectra of complexes **1a**, **1b**, **2b**, and **3** to **5** in THF. The inset in the top spectrum shows a linear relation between the energy of the CT absorption band (ν_{CT}) in MeCy and the oxidation potential (E_{ox}) of the complexes. The crystal structures of complexes **1b** and **2b** are shown as insets in the bottom

spectrum. The pendant adamantyl and Dipp groups are depicted in wire-frame for clarity. (B) Blue shift of the ICT absorption band with increasing solvent polarity observed in complexes **1a** and **5**. (C) Absorption spectra of complex **1a** at room temperature (RT) and 77 K, showing a blue shift in the ICT band at low temperature. a.u., arbitrary units.

Table 1. Photophysical data for complexes 1a, 1b, 2b, and 3 to 5 doped 1% by weight into PS films or dissolved at 10^{-5} M concentration in 2-MeTHF. n.d., not determined.

Complex	Emission at room temperature					Emission at 77 K	
	λ_{max} (nm)	τ (μs)	Φ_{PL}	k_r (s^{-1})	k_{nr} (s^{-1})	λ_{max} (nm)	τ (μs)
1% weight PS films							
1a	474	2.8	1.0	3.5×10^5	3.6×10^3	480	64
3	426	240 (70%) 1300 (30%)	0.82	1.5×10^3	3.2×10^2	424	6900
4	518	2.3	1.0	4.3×10^5	$<4.4 \times 10^3$	490	550
5	532	2.6	0.78	3.0×10^5	8.5×10^4	536	264
2-MeTHF							
1a	492	2.5	1.0	3.9×10^5	$<8.0 \times 10^3$	430	7300
1b	510	2.3	0.68	3.0×10^5	1.7×10^5	430	430 nm: 3000 500 nm: 48
1c	500	1.8	0.56	3.1×10^5	2.4×10^5	430	7000
1d	510	0.54	0.11	2.0×10^5	1.6×10^6	430	5000
2b	542	0.86 (79%) 2.3 (21%)	0.12	$1.1 \times 10^{5*}$	$8.0 \times 10^{5*}$	438	430 nm: 2400 500 nm: 37
3	428 590 [†]	450 nm: 8.3 600 nm: 8.0	0.11	n.d.	n.d.	422	12,000
4	558	0.28	0.25	8.9×10^5	2.7×10^6	470	Seconds
5	580	0.87	0.16	1.8×10^5	9.7×10^6	500	215

*Calculated from a weighted average of the two contributions to τ . †Excimer peak.

radiative rate constants ($k_r = 2.0 \times 10^5$ to $4.3 \times 10^5 \text{ s}^{-1}$), the principal effect of increasing steric bulk is to decrease the rates of nonradiative decay. Complexes **4** and **5** show red-shifted emission relative to complex **1a**, with radiative rates comparable to that of **1a** (Table 1). The sparingly soluble complex **3** shows narrow, structured emission centered at 426 nm in solution and has a radiative rate constant that is lower than the other complexes, features we attribute to emission from a state with predominant triplet-carbazolide (^3Cz) character, vide infra (Fig. 3D). In addition, complex **3** displays a low energy ($\lambda \sim 600 \text{ nm}$) concentration-dependent emission band in solution, characterized by a rise time in its PL decay traces (see fig. S34 and table S17), which is consistent with the diffusional process required to form a luminescent excimer.

To eliminate the complications of aggregation and excimer formation in photophysical studies, we doped the complexes into thin films [1 weight

% in PS], where excimer formation is suppressed. At room temperature, samples in the rigid matrix exhibit a blue shift in their emission relative to spectra recorded in solution (i.e., rigidochromism) and suppressed rates of nonradiative decay (Fig. 3A). Complexes **1a** and **4** display broad emission with near unity quantum efficiency in PS ($\Phi_{\text{PL}} = 1.0$), whereas complex **5** is less efficient ($\Phi_{\text{PL}} = 0.78$) (Table 1). Thin films of complex **3** give narrow, structured emission at room temperature with biexponential decay lifetimes of 240 μs and 1.3 ms. The slow radiative rates in **3** ($k_r = 1.5 \times 10^3 \text{ s}^{-1}$) are consistent with our initial ^3Cz assignment, owing to the highly destabilized ICT in this complex (Fig. 3D). Notably, the high Φ_{PL} and k_r values for complexes **1a**, **4**, and **5** in solution and thin films are comparable to phosphors containing heavy metals, such as Ir and Pt.

The photoluminescent properties are dramatically altered on cooling to 77 K. A vibronically

structured, long-lived emission (τ of ms to s, $k_r < 10^3 \text{ s}^{-1}$) is observed for **1a** to **1d**, **3**, and **4** in frozen glasses of 2-MeTHF and MeCy (Table 1 and Fig. 3B). The emission at 77 K is assigned to a low-lying triplet state localized on the carbazolide ligand (^3Cz), as the phosphorescence spectrum of KCz in frozen 2-MeTHF replicates the same profile as **1a** (Fig. 3B). The blue shift in emission observed in MeCy at 77 K corresponds with the hypsochromic shift observed in ICT absorption at that temperature, as destabilizing the ICT transition leaves ^3Cz as the lowest-lying emissive state (Fig. 3E). Luminescence from **5** is broad and featureless in frozen glassy matrices, with long excited-state lifetimes ($\tau = 215 \mu\text{s}$ in 2-MeTHF), consistent with emission from a ^3ICT state (Fig. 3D).

The luminescent properties of **1a** and **5** in thin PS films were examined as a function of temperature to probe the ICT manifold while avoiding complications from ^3Cz -dominated emission

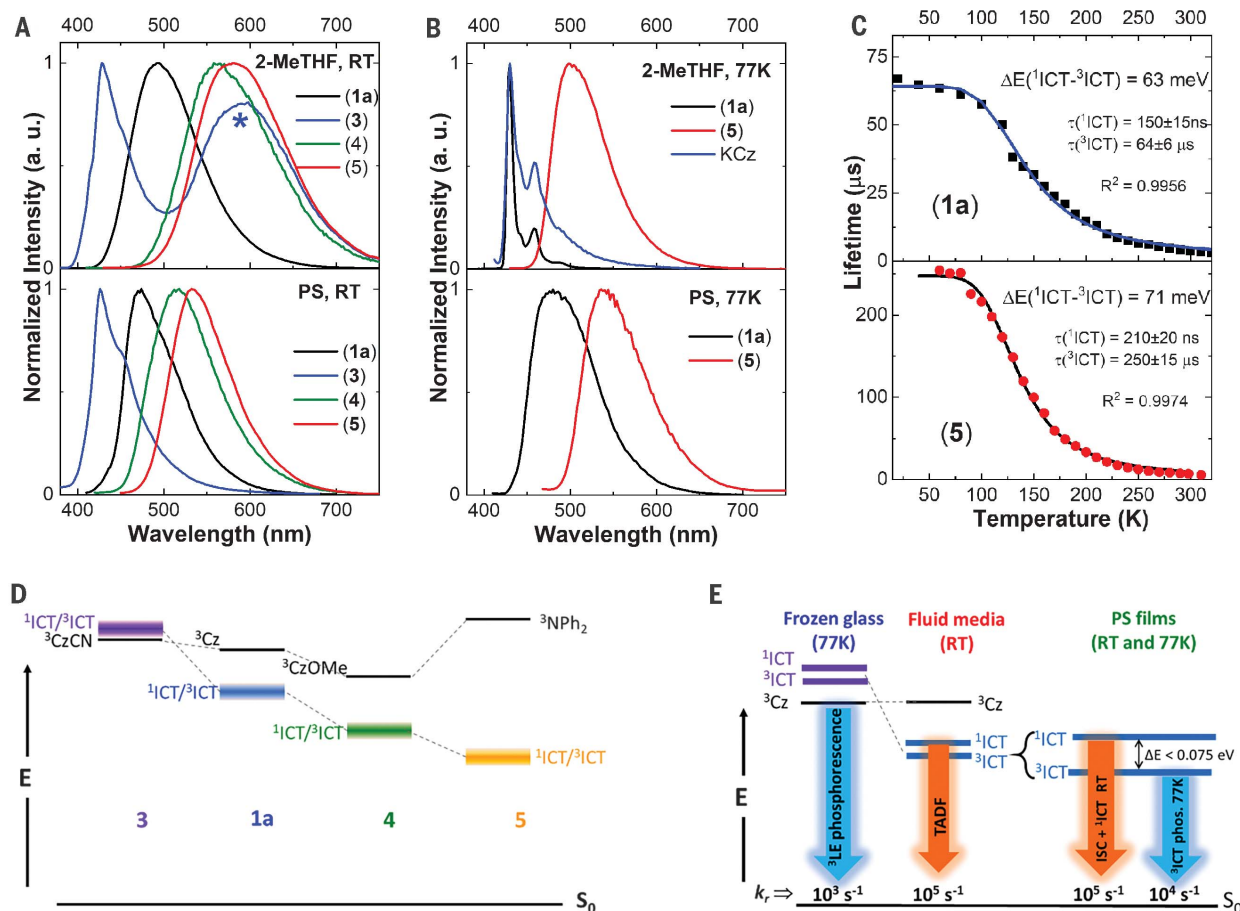


Fig. 3. Luminescence behavior of CAAC-Cu-amides. (A) Room-temperature emission spectra of complexes **1a** and **3** to **5** at 10^{-5} M in 2-MeTHF and doped 1% by weight into PS films. The asterisk indicates excimer emission. (B) 77 K emission spectra of complexes **1a** and **5** in 2-MeTHF (10^{-5} M) and 1% PS films. Also shown is the gated phosphorescence spectrum of KCz at 77 K (top). (C) Temperature-dependent PL decays of complexes **1a** (top)

and **5** (bottom) as well as the data fit to Eq. 1. The parameters obtained from the fit, $\Delta E_{\text{ICT}-^3\text{CT}}$, τ_{ICT} , and τ_{ICT} , are shown in each plot. (D) State diagram depicting $^1\text{Cz}^*/^3\text{Cz}^*$ ordering in the reported complexes. The relative energies of the states are based on emission spectra. (E) Jablonski diagram depicting the different processes operating in various media at room temperature and 77 K.

in frozen solvents. Temperature-dependent emission of thin PS films of both complexes display broad, featureless ICT spectra at all temperatures between 10 and 300 K (see figs. S30 and S31) and have excited state lifetimes that increase with decreasing temperatures (Fig. 3C). Fits of the temperature-dependent PL decay curve to a Boltzmann distribution (Eq. 1) give $\Delta E_{i_{CT-3CT}} = 0.063$ eV (510 cm^{-1}) for **1a** and 0.071 eV (570 cm^{-1}) for **5** [coefficient of determination (R^2) values for the fits of **1a** and **5** in Fig. 3C are 0.996 and 0.997, respectively]. The radiative lifetimes of ^1ICT (**1a**, $\tau = 150 \pm 15$ ns; **5**, $\tau = 210 \pm 21$ ns) and ^3ICT (**1a**, $\tau = 64 \pm 6$ μs ; **5**, $\tau = 250 \pm 15$ μs), derived from the fits to Eq. 1, are comparable to values reported by Yersin and co-workers and Bräse and co-workers in the fastest Cu(I) TADF emitters reported to date (22, 38). The rate of emission at low temperature attributed to ^3ICT -based phosphorescence is faster for **1a** than for **5**, owing to the close-lying ^3Cz in **1a**, which can enhance SOC by mixing with ^3ICT through configuration interaction (9, 12).

We also investigated the role of ligand conformation in the photophysical properties using complexes **1b** and **2b**: The former has coplanar orientation of carbene and carbazole ligands, whereas the ligands are nearly orthogonal in the latter. The ICT absorption band in **2b** has an extinction coefficient reduced threefold relative to **1b**: $\epsilon_{\text{ICT}} = 1300$ and 4000 $\text{M}^{-1} \text{cm}^{-1}$, respec-

tively (Fig. 2A). Similarly, the efficiency and radiative rate constant for **2b** are reduced nearly fourfold relative to **1b** ($\Phi_{\text{PL}} = 0.12$ and 0.68 , and $k_r = 1.1 \times 10^5$ and 3×10^5 s^{-1} , respectively). The marked decrease in k_r observed for **2b** is important in light of the decrease in HOMO-LUMO overlap and the expected decrease in $\Delta E_{i_{CT-3CT}}$ (35). These observations highlight the impact of a coplanar ligand conformation on maintaining the strongly allowed nature of the ICT transitions in absorption and emission and are therefore incompatible with the rotationally accessed spin-state inversion (RASI) mechanism described by Di *et al.* (19), as previously noted by Föller and Marian and Penfold and co-workers (35, 39). Moreover, the suggestion by Di *et al.* that the S_1 state lies below the T_1 state in energy when the carbene and carbazole ligands are orthogonal is not supported by these experimental results and is counter to what is expected on the basis of fundamental quantum mechanical considerations (40).

Time-dependent DFT (TDDFT) was used to model the main electronic transitions of the excited states in these complexes (see the supplementary materials for details). The ^3ICT state shares the same orbital parentage as ^1ICT and lies within 0.25 eV of the latter (table S22), in agreement with recent reports from Föller and Marian (35) and Tafett *et al.* (41). In addition, the ^3Cz state is only 0.03 to 0.1 eV higher in en-

ergy than the ^3ICT state in all the carbazolidone-based complexes except for **3**, where it is the lowest triplet state. The triplet state localized on the diphenylamide in **5**, ^3LE (i.e., $^3\text{NPh}_2$), is destabilized relative to ^3ICT by 0.5 eV.

We have further modeled the effects of solvation on the excited states of complex **1a** at 77 and 300 K using a multiscale hybrid approach that used molecular dynamics simulations in conjunction with TDDFT, as detailed in the supplementary materials. At room temperature, it was found that the ^3ICT state is the lowest triplet state in all cases owing to stabilization by the solvent dipoles (fig. S41). A similar procedure was followed to study the effect of solvation at 77 K, where single-point TDDFT calculations were performed on a frozen equilibrated cell using the hybrid scheme described in the supplementary materials. Here it was found that the ^3Cz state is the lowest-lying triplet, in accordance with the experimental observation of ^3Cz emission in 2-MeTHF at 77 K. The destabilization of the ^3ICT state can be attributed to its associated dipole (4.25 D), which is opposite in direction to the large dipole in the ground ^1ICT (11.8 D) and ^3Cz states (11.27 D). Hence, solvent molecules in a frozen matrix are expected to be ordered so as to stabilize the ground state, whereas the ^3CT state would be destabilized. Negative solvatochromic effects observed in absorption can be explained by the same rationale.

Exploration of CAAC-Cu-amides as emitters in blue OLEDs

OLEDs incorporating **1a** as an emitter were fabricated by vapor deposition (see the supplementary materials for details), following the general architecture outlined in Fig. 4A and only changing the emissive layer to screen different wide bandgap host materials. Commonly used hosts in blue OLEDs [1,3-bis(triphenylsilyl)benzene (UGH3); 3,3'-bis(carbazol-9-yl)biphenyl (mCBP); and dicarbazolyl-3,5-benzene (mCP)] were examined. In addition, we also tried a Cu-based host, that is, (CAAC)Cu-C₆F₅, with a high triplet energy; however, these devices degraded rapidly during operation (see the supplementary materials). Thin films doped into the various established hosts show similar trends with Φ_{PL} in UGH3 > mCBP > mCP (0.9, 0.6, and 0.3 respectively). OLEDs prepared with **1a** doped into UGH3 at 20 volume % give $\text{EQE}_{\text{max}} = 9.0\%$ and 16 cd/A at 2 mA/cm^2 (Fig. 4B), consistent with the high triplet energy of the UGH3 host ($T_1 = 3.5$ eV). Although the EQE values for green- and yellow- or orange-emitting Cu-based OLEDs have been reported to be >20% (42, 43), the highest efficiencies previously reported for blue-emitting ($\text{EL } \lambda_{\text{max}} < 500$ nm) Cu-based OLEDs are <6% (44, 45). The low EQE_{max} of the mCBP and mCP devices can be explained by a low triplet energy for the hosts (mCBP, $T_1 = 2.8$ eV; mCP, $T_1 = 2.9$ eV), which do not confine triplet excitons on the Cu emitter as efficiently as UGH3. The roll-off in device efficiency as the current is raised for the UGH3-based device (Fig. 4B) is

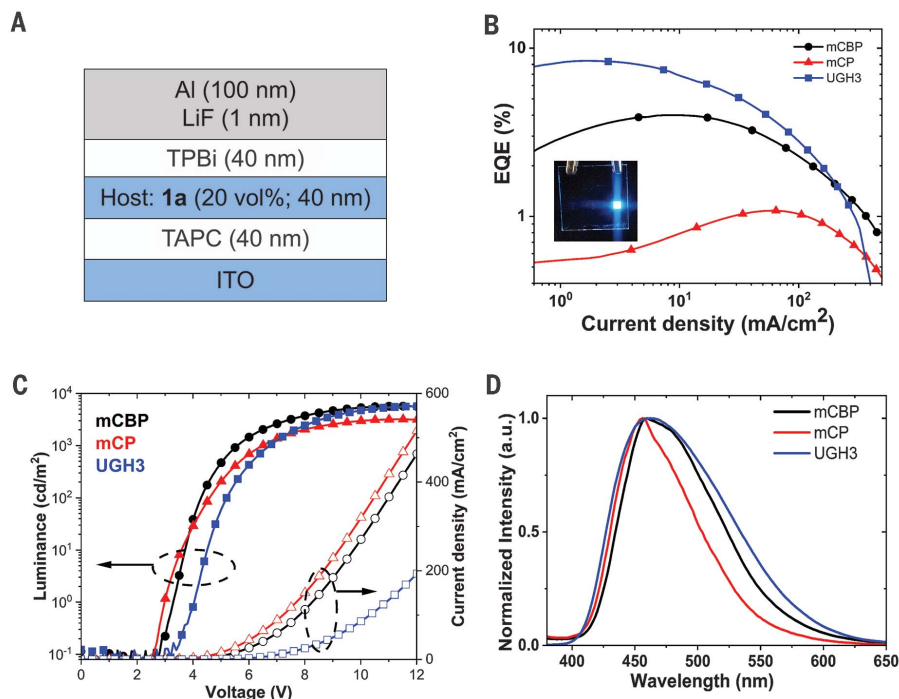


Fig. 4. OLED demonstration. (A) OLED device architecture energy scheme for **1a**-based OLEDs. TPBi, 2,2',2''-(1,3,5-benzinetriyl)-tris(1-phenyl-1-*H*-benzimidazole); TAPC, 4,4'-cyclohexylidenebis[*N,N*-bis(4-methylphenyl)benzenamine]; ITO, indium tin oxide. (B) EQE traces of devices using different hosts. The inset is a photograph of a **1a**-based device. (C and D) Current (J)-voltage (V)-luminance (L) traces (C) and EL spectra (D) of devices using different hosts.

comparable to the roll-off observed for UGH3-based OLEDs with an iridium-based emitter (46), which has been attributed to increased triplet-triplet and triplet-polaron annihilation at higher current density (47, 48). All devices exhibit blue EL, similar to the PL for **1a** in a PS film, with minor shifts due to “solvent” effects of the different host matrices. This is in contrast to the green-emissive OLEDs reported by Di *et al.* (19) for an OLED with **1b** doped into polyvinylcarbazole. We expect that stable, high-triplet energy host materials for blue OLEDs using emitter **1a** should positively affect both efficiency and device stability.

Outlook

We have prepared a series of two-coordinate CAAC-Cu-amide complexes with emission tunable across the visible spectrum, high Φ_{PL} (up to >99%) in nonrigid media, and $k_r > 10^5 \text{ s}^{-1}$. Emission stems from a strongly allowed amide-to-carbene ICT transition, with the coplanar ligand conformation and coupling through the metal d orbitals ensuring strong ϵ_{ICT} and resultant k_r . By contrast, a near-orthogonal arrangement of ligands leads to both low ϵ_{ICT} and a decrease in k_r owing to poor orbital overlap. In the Cu-carbazolide complexes, there exists a closely lying ^3Cz -centered state that dominates emission in frozen solvent glasses, owing to the destabilization of the ICT manifold in such media. Within the ICT manifold, efficient TADF is observed with $\Delta E_{\text{CT}}^{\text{ICT}} < 75 \text{ meV}$, among the smallest values recorded for mononuclear Cu(I)-based TADF systems (49).

The τ_{ICT} values we obtain are typical in Cu(I) TADF-based emitters; however, they are far longer than the prompt fluorescence rates recorded in pure organic TADF systems, with τ_{f} values on the order of 10 ns (50). Another distinction from organic TADF systems is the much longer-lived (millisecond to second) phosphorescence at low temperature for organics. The discrepancy between organometallic and organic TADF suggests that a spin-pure treatment of the CT manifold is inadequate in organometallic emitters, owing to stronger SOC effects (51). The slow ^1CT decay in Cu-based systems is likely due to considerable mixing with ^3ICT via SOC. The opposite is true for ^3ICT , where considerable singlet character in the nominally triplet state leads to markedly faster decay than expected for a spin-pure triplet. The acronym TADF is an imprecise description for what is observed in Cu-based complexes of the type described here, because neither the singlet nor triplet states are spin-pure. Lifetimes as high as 0.2 μs for the ^1CT state suggest that this state has substantial triplet contribution, thus fluorescence is not the best description for this type of emission (51, 52). The process observed here is better described as thermally enhanced luminescence, where both the lower-energy and higher-energy states are highly emissive, albeit with the lower state having a much longer radiative lifetime. Thermal enhancement here manifests in a shortening of the radiative lifetime but does not markedly increase the already high luminance efficiency.

The extent of Cu involvement in the electronic properties of these complexes appears to be the answer to the Cu-TADF conundrum we posited: The metal contribution is large enough to induce high exo- and endothermic k_{ISC} , yet low enough to ensure small reorganization energies. This work outlines the design parameters for attaining Cu(I) complexes with photophysical properties akin to their heavy metal counterparts: maintaining a two-coordinate geometry around the metal center, with redox-active ligands in a coplanar orientation. These results therefore open the door to investigation of these complexes in fields where traditional heavy metal-based phosphors have been used, for example, optical sensing, photoredox catalysis, and solar fuel generation, to name a few.

REFERENCES AND NOTES

- K. Kalyanasundaram, *Coord. Chem. Rev.* **46**, 159–244 (1982).
- M. H. Keefe, K. D. Benkstein, J. T. Hupp, *Coord. Chem. Rev.* **205**, 201–228 (2000).
- K. K.-W. Lo, M.-W. Louie, K. Y. Zhang, *Coord. Chem. Rev.* **254**, 2603–2622 (2010).
- M. Grätzel, *Inorg. Chem.* **44**, 6841–6851 (2005).
- S. Lamansky *et al.*, *J. Am. Chem. Soc.* **123**, 4304–4312 (2001).
- H. J. Bolink, E. Coronado, R. D. Costa, N. Lardiés, E. Ortí, *Inorg. Chem.* **47**, 9149–9151 (2008).
- P. C. Ford, A. Vogler, *Acc. Chem. Res.* **26**, 220–226 (1993).
- N. Armaroli, G. Accorsi, F. Cardinali, A. Listorti, in *Photochemistry and Photophysics of Coordination Compounds I*, V. Balzani, S. Campagna, Eds. (Springer, 2007), pp. 69–115.
- H. Yersin, A. F. Rausch, R. Czerwiec, T. Hofbeck, T. Fischer, *Coord. Chem. Rev.* **255**, 2622–2652 (2011).
- S. Fraga, K. M. S. Saxena, J. Karwowski, *Handbook of Atomic Data*. Physical Science Data (Physical Science Data Series, vol. 5, Elsevier, 1976).
- L. Bergmann, G. J. Hedley, T. Baumann, S. Bräse, I. D. W. Samuel, *Sci. Adv.* **2**, e1500889 (2016).
- T. J. Penfold, E. Gindensperger, C. Daniel, C. M. Marian, *Chem. Rev.* **118**, 6975–7025 (2018).
- G. J. Hedley, A. Ruseckas, I. D. W. Samuel, *Chem. Phys. Lett.* **450**, 292–296 (2008).
- M. Kleinschmidt, C. van Wüllen, C. M. Marian, *J. Chem. Phys.* **142**, 094301 (2015).
- J. Brooks *et al.*, *Inorg. Chem.* **41**, 3055–3066 (2002).
- S. Lamansky, R. C. Kwong, M. Nugent, P. I. Djurovich, M. E. Thompson, *Org. Electron.* **2**, 53–62 (2001).
- Z. A. Siddique, Y. Yamamoto, T. Ohno, K. Nozaki, *Inorg. Chem.* **42**, 6366–6378 (2003).
- H. Uoyama, K. Goushi, K. Shizu, H. Nomura, C. Adachi, *Nature* **492**, 234–238 (2012).
- D. Di *et al.*, *Science* **356**, 159–163 (2017).
- H. Yersin, R. Czerwiec, M. Z. Shafikov, A. F. Suleymanova, *ChemPhysChem* **18**, 3508–3535 (2017).
- H. Yersin, Ed., *Highly Efficient OLEDs: Materials Based on Thermally Activated Delayed Fluorescence* (Wiley, 2019).
- R. Czerwiec, M. J. Leitl, H. H. H. Homeier, H. Yersin, *Coord. Chem. Rev.* **325**, 2–28 (2016).
- J. R. Kirchhoff *et al.*, *Inorg. Chem.* **22**, 2380–2384 (1983).
- R. Czerwiec, J. Yu, H. Yersin, *Inorg. Chem.* **50**, 8293–8301 (2011).
- P. K. Samanta, D. Kim, V. Coropceanu, J.-L. Brédas, *J. Am. Chem. Soc.* **139**, 4042–4051 (2017).
- M. Iwamura, H. Watanabe, K. Ishii, S. Takeuchi, T. Tahara, *J. Am. Chem. Soc.* **133**, 7728–7736 (2011).
- C. E. McCusker, F. N. Castellano, *Inorg. Chem.* **52**, 8114–8120 (2013).
- M. Gernert, U. Müller, M. Haehnel, J. Pflaum, A. Steffen, *Chemistry* **23**, 2206–2216 (2017).
- S. Shi *et al.*, *Dalton Trans.* **46**, 745–752 (2017).
- R. Hamze *et al.*, *Chem. Commun. (Camb.)* **53**, 9008–9011 (2017).

- M. Melaimi, R. Jazzar, M. Soleilhavoup, G. Bertrand, *Angew. Chem. Int. Ed.* **56**, 10046–10068 (2017).
- O. Back, M. Henry-Ellinger, C. D. Martin, D. Martin, G. Bertrand, *Angew. Chem. Int. Ed.* **52**, 2939–2943 (2013).
- M. M. Hansmann, M. Melaimi, D. Munz, G. Bertrand, *J. Am. Chem. Soc.* **140**, 2546–2554 (2018).
- D. C. Rosenfeld, P. T. Wolczanski, K. A. Barakat, C. Buda, T. R. Cundari, *J. Am. Chem. Soc.* **127**, 8262–8263 (2005).
- J. Föllner, C. M. Marian, *J. Phys. Chem. Lett.* **8**, 5643–5647 (2017).
- C. Reichardt, *Chem. Rev.* **94**, 2319–2358 (1994).
- V. Bulović, R. Deshpande, M. E. Thompson, S. R. Forrest, *Chem. Phys. Lett.* **308**, 317–322 (1999).
- D. Volz *et al.*, *Chem. Mater.* **25**, 3414–3426 (2013).
- S. Thompson, J. Eng, T. J. Penfold, *J. Chem. Phys.* **149**, 014304 (2018).
- S. P. McGlynn, T. Azumi, M. Kinoshita, *Molecular Spectroscopy of the Triplet State* (Prentice-Hall, Inc., 1969).
- E. J. Taffet, Y. Olivier, F. Lam, D. Beljonne, G. D. Scholes, *J. Phys. Chem. Lett.* **9**, 1620–1626 (2018).
- Y. Liu, S.-C. Yiu, C.-L. Ho, W.-Y. Wong, *Coord. Chem. Rev.* **375**, 514–557 (2018).
- M. Wallech *et al.*, in *Proceedings SPIE 9183, Organic Light Emitting Materials and Devices XVIII*, F. So, C. Adachi, Eds. (SPIE, 2014), 918309.
- D. Liang *et al.*, *Inorg. Chem.* **55**, 7467–7475 (2016).
- X.-L. Chen *et al.*, *Chem. Mater.* **25**, 3910–3920 (2013).
- X. Ren *et al.*, *Chem. Mater.* **16**, 4743–4747 (2004).
- S. Reineke, K. Walzer, K. Leo, *Phys. Rev. B* **75**, 125328 (2007).
- L. Zhang, H. van Eersel, P. A. Bobbert, R. Coehoorn, *Chem. Phys. Lett.* **652**, 142–147 (2016).
- M. Osawa *et al.*, *J. Mater. Chem. C Mater. Opt. Electron. Devices* **1**, 4375–4383 (2013).
- P. L. Santos *et al.*, *J. Mater. Chem. C Mater. Opt. Electron. Devices* **4**, 3815–3824 (2016).
- R. Baková, M. Chergui, C. Daniel, A. Vlček Jr., S. Zális, *Coord. Chem. Rev.* **255**, 975–989 (2011).
- N. J. Turro, *Modern Molecular Photochemistry* (University Science Books, 1991).

ACKNOWLEDGMENTS

Funding: This work was supported by the Universal Display Corporation for the University of Southern California authors; a National Science Foundation (NSF) Graduate Research Fellowship (grant no. DGE-1650112) supported J.L.P.; and the NSF (CHE-1661518) supported all UCSD authors. Computation for the work described in this paper was supported by the University of Southern California’s Center for High-Performance Computing (<https://hpcc.usc.edu/>). **Author contributions:** R.Ham., J.L.P., J.C. M.S., and R.J. synthesized and characterized the compounds, R.Ham. collected and analyzed the spectroscopic data. M.J. and R.Ham. fabricated and tested the OLEDs. R.Ham., J.L.P., R.J., and R.Hai. determined the x-ray structures. D.S. performed the theoretical calculations. R.Ham., P.I.D., and M.E.T. wrote the manuscript. G.B. and M.E.T. directed the project. **Competing interests:** R.Ham., M.J., P.I.D., and M.E.T. are inventors on a patent application submitted by the University of Southern California based partly on the intellectual property in this report. One of the authors (M.E.T.) has a financial interest in the Universal Display Corporation. **Data and materials availability:** Structural data for all of the copper complexes reported here are freely available from the Cambridge Crystallographic Data Centre (CCDC nos. 1865272 to 1865277 for **1a**, **1c**, **1d**, and **3** to **5**; CCDC no. 1857183 for **2b**; and CCDC no. 1861278 for **Cu Host**). The supplementary materials for this paper include synthetic and characterization data (^1H and ^{13}C NMR spectra, mass spectrometry, and elemental analysis) for each copper complex; electrochemical data, ORTEP drawings, and crystallographic information on the compounds listed above; photophysical data; and details of DFT, TDDFT, and molecular dynamics calculations.

SUPPLEMENTARY MATERIALS

www.sciencemag.org/content/363/6427/601/suppl/DC1
Materials and Methods
Figs. S1 to S61
Tables S1 to S22
References (53–69)

2 September 2018; accepted 2 January 2019
10.1126/science.aav2865

Eliminating nonradiative decay in Cu(I) emitters: >99% quantum efficiency and microsecond lifetime

Rasha Hamze, Jesse L. Peltier, Daniel Sylvinson, Moonchul Jung, Jose Cardenas, Ralf Haiges, Michele Soleilhavoup, Rodolphe Jazzar, Peter I. Djurovich, Guy Bertrand and Mark E. Thompson

Science **363** (6427), 601-606.
DOI: 10.1126/science.aav2865

Helping copper glow

Copper's abundance makes the metal an appealing candidate for luminescence applications. However, many copper complexes tend to decay nonradiatively after photoexcitation. A recently described exception involves a two-coordinate complex that sandwiches the metal between an amide ligand and a carbene ligand. Hamze *et al.* thoroughly explored this motif and measured a nearly perfect luminescence efficiency. They used this property to produce a prototype blue organic light-emitting diode. The photodynamics appeared largely ligand-centered, with the excited state attributed to copper-facilitated charge transfer from amide to carbene.

Science, this issue p. 601

ARTICLE TOOLS

<http://science.sciencemag.org/content/363/6427/601>

SUPPLEMENTARY MATERIALS

<http://science.sciencemag.org/content/suppl/2019/02/06/363.6427.601.DC1>

REFERENCES

This article cites 62 articles, 2 of which you can access for free
<http://science.sciencemag.org/content/363/6427/601#BIBL>

PERMISSIONS

<http://www.sciencemag.org/help/reprints-and-permissions>

Use of this article is subject to the [Terms of Service](#)